

Numerical sub-gap spectroscopy of double quantum dots coupled to superconductors: supplementary information

Rok Žitko^{1,2}

¹Jožef Stefan Institute, Jamova 39, SI-1000 Ljubljana, Slovenia

²Faculty of Mathematics and Physics, University of Ljubljana, Jadranska 19, SI-1000 Ljubljana, Slovenia

I. SINGLE QUANTUM DOT: SUPERCONDUCTING STATE

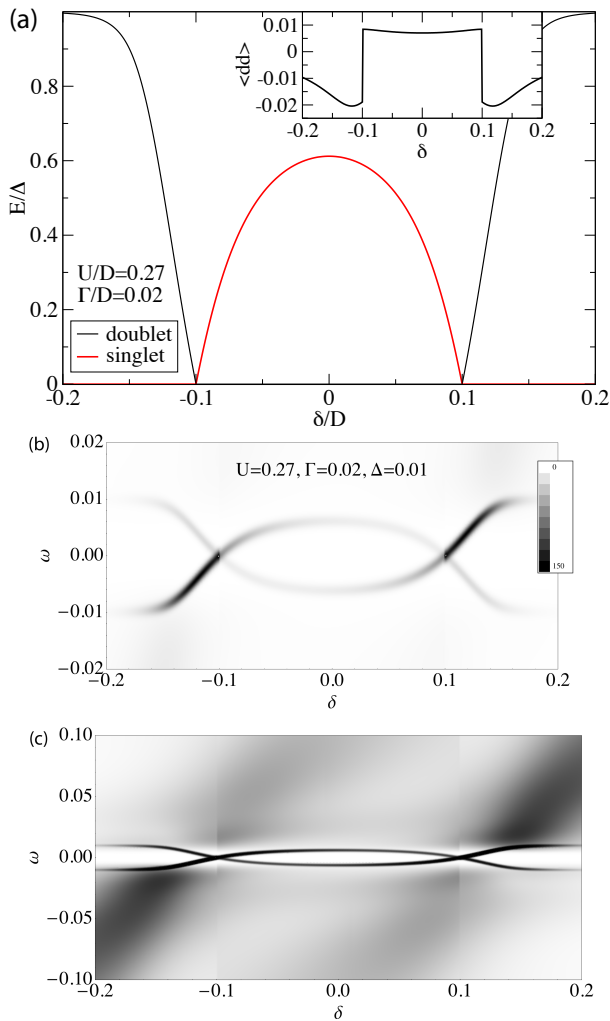


Figure 1: (Color online) Single quantum dot coupled to a superconducting lead. (a) Sub-gap ($\omega < \Delta$) part of the many-particle excitation spectrum which includes one spin-singlet and one spin-doublet. The energies are plotted by subtracting the ground-state energy, thus the lowest lying state is always at $E = 0$. The continuum of quasiparticle states extends from $E = \Delta$ upwards. The inset shows the ground-state expectation value of the pairing operator, $\langle d_{\uparrow}d_{\downarrow} \rangle$, whose sign reveals the type of the ground state. (b) The corresponding impurity spectral function, measurable through tunneling spectroscopy. (c) Spectral function in an extended frequency range plotted using a nonlinear grayscale to emphasize the low-intensity details outside the gap.

For parameters from the main text, T_K is lower than Δ close to half filling, the local moment remains unscreened and the ground state is a spin doublet, see Fig. 1(a). T_K increases with increasing $|\delta|$ until at $|\delta| \approx 0.1$ the condition

$$T_K(\delta) \approx 0.3\Delta \quad (1)$$

is satisfied and the new ground state is the spin singlet. This level crossing is accompanied by discontinuities in all physical properties, for instance in the expectation value of the local pairing operator $\langle d_{\uparrow}d_{\downarrow} \rangle$ (inset to panel a) and in the spectral function (panels b and c). The spectral function is defined as

$$A(\omega) = \frac{1}{Z} \sum_{i,j} [\exp(-\beta E_i) + \exp(-\beta E_j)] \times (\langle i|d_{\sigma}^{\dagger}|j \rangle)^2 \delta[\omega - (E_j - E_i)], \quad (2)$$

with $Z = \sum_i \exp(-\beta E_i)$, i and j run over all many-particle states and $\beta = 1/k_B T$. The only sub-gap excitation that contributes to $A(\omega)$ at zero temperature is the transition from singlet to doublet state (or vice versa), which produces a pair of peaks at $\omega = \pm(E_D - E_S)$. The total weight of these peaks depends on δ and varies discontinuously across the transition. The spectrum above and around the gap edges features atomic peaks at $\omega \approx \epsilon$ and $\omega \approx \epsilon + U$ which fuse with the superconducting coherence peaks at $|\omega| = \Delta$. This occurs close to (but not exactly at) the singlet-doublet quantum phase transition points.

II. DOUBLE QUANTUM DOT: NORMAL STATE

A. Left-right particle-hole symmetric case

At half filling the Kondo screening competes with the inter-dot superexchange coupling $J = 4t^2/U$. The spectrum is shown in Fig. 2. For small t , it is the same as in the single-impurity case, with broad peaks at $\omega = \pm U/2$ and a Kondo resonance at $\omega = 0$. The low-frequency part of the spectrum starts to be affected by the superexchange interaction for t such that $J \sim T_K$. For our parameters this occurs at $t \sim 10^{-2}$. The behavior in this range is governed by the proximity of the two-impurity Kondo model (TIKM) non-Fermi-liquid fixed point^{1,2}. For $t \gtrsim 10^{-2}$ the Kondo peak amplitude is reduced and a splitting of order $J \propto t^2$ becomes observable. As t increases further, the hybridization between the local orbitals becomes the dominant effect, resulting in the splitting between the anti-bonding and bonding molecular orbitals that is linear in t . This occurs at $t \sim 10^{-1}$. The Kondo, the anti-ferromagnetic, and the molecular-orbital regimes can be even

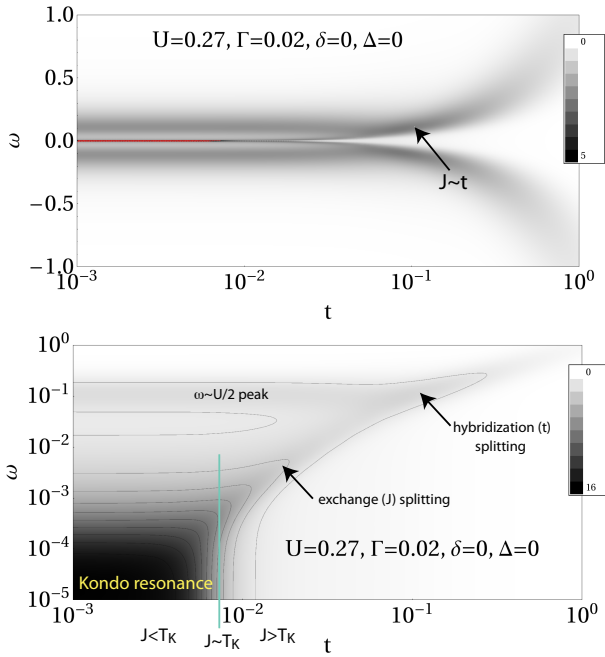


Figure 2: (Color online) Spectral function on one of the dots, $A_1(\omega)$, in the left-right symmetric DQD system in the *normal state* with linear (upper panel) and logarithmic (bottom panel) frequency scales.

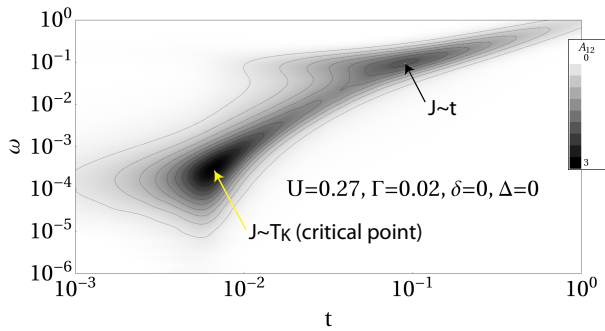


Figure 3: (Color online) Interdot spectral function $A_{12}(\omega)$ in the left-right symmetric DQD system in the *normal state* with logarithmic frequency scale. This spectral function is odd in frequency, thus we only show $\omega > 0$. The enhancement of $A_{12}(\omega)$ at $\omega \sim T_K$, which occurs for $t \approx 9 \times 10^{-3}$, indicates the two-impurity Kondo model critical point, and the enhancement at $\omega \sim 0.1 \approx t$ indicates the transition to the molecular-orbital regime.

more clearly distinguished in the inter-impurity spectral function $A_{12}(\omega)$ shown in Fig. 3. The plot on the logarithmic scale allows easy identification of the cross-over scales defined by $J \sim T_K$ and $J \sim t$, respectively. The change of slope of the main ridge in $A_{12}(\omega)$ from quadratic to linear directly reveals the cross-over of the main coupling mechanism from the superexchange interaction to the hybridization (bonding) effects.

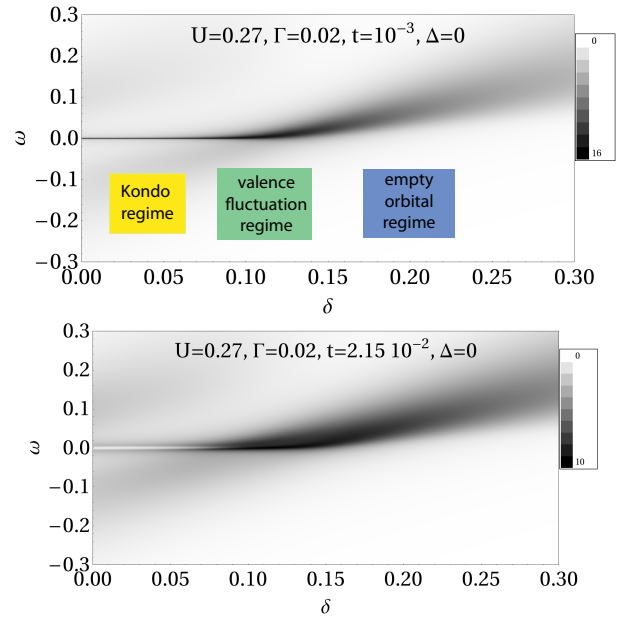


Figure 4: (Color online) Spectral function $A_1(\omega)$ in the left-right symmetric DQD system away from half-filling. (a) Small coupling $t = 10^{-3}$, (b) intermediate coupling $t = 2.15 \times 10^{-2}$.

B. Away from particle-hole symmetry

We maintain the left-right symmetry, but move away from the half filling. For low inter-dot coupling t , the behavior mirrors that of single dots, see Fig. 4, top panel. With increasing δ the atomic peaks shift to higher energies and the width of the Kondo resonance increases as T_K grows. This continues until $\delta \approx U/2 - \Gamma \approx 0.1$ when the system enters the valence fluctuation regime and the Kondo resonance merges with the lower atomic peak. For even larger δ , the system is in the empty orbital regime with no electrons occupying the quantum dot. For larger t the spectra are similar, but an exchange splitting becomes visible in the Kondo regime, see Fig. 4, bottom panel.

C. Fully generic case

To study the fully generic case with different on-site energies δ_i , we fix δ_2 and plot the sweeps of δ_1 for different values of the inter-dot coupling t . At $\delta_2 = 0$, the dot 2 is half filled and thus in the Kondo regime. At large enough t the exchange coupling J starts to influence the spectra. The results for $t = 10^{-2}$ are shown in the top row in Fig. 5. For small δ_1 we observe on both dots the expected exchange splitting of the Kondo resonance. T_K on dot 1 increases with increasing δ_1 . Near $\delta_1 = 0.07$, the condition $J \sim T_K$ is fulfilled, as revealed by the disappearance of splitting in $A_2(\omega)$ for $\delta_1 > 0.07$. The splitting in $A_1(\omega)$ persists to higher values of δ_2 , even in the valence fluctuation regime of dot 1 at $\delta_1 \approx U/2 - \Gamma$. A closer inspection of the results reveals that the splitting in this regime corresponds to the width of the Kondo resonance on dot 2.

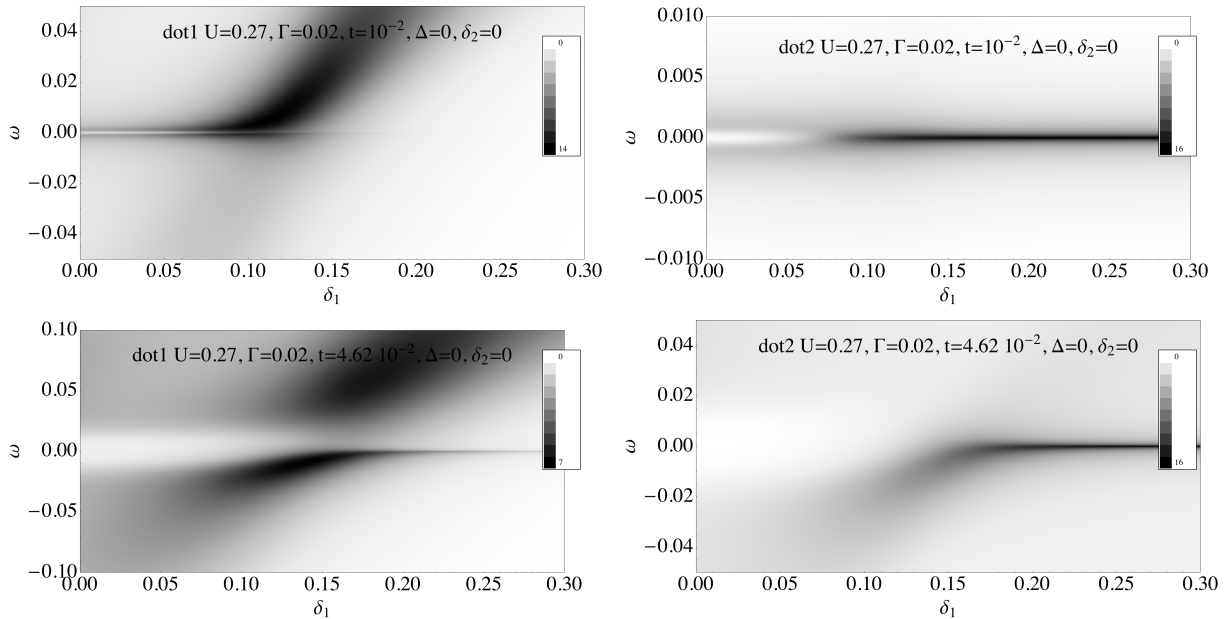


Figure 5: (Color online) Spectral function on dot 1 (left panels) and dot 2 (right panels) for two values of the inter-dot couplings t . The quantum dot 2 is kept at $\delta_2 = 0$, which is the *Kondo regime*.

This splitting is thus not due to the exchange coupling, but is a simple coherence (proximity) effect due to particle hopping between the dots. Spectral dips of similar magnitude can thus be generated by quite different mechanisms.

At larger $t = 4.62 \times 10^{-2}$, the effects of the inter-dot tunneling become even more pronounced, see the bottom row in Fig. 5. The two dots behave increasingly as a single entity, thus there is a pronounced “mirroring” of spectral features in $A_1(\omega)$ and $A_2(\omega)$. The most pronounced effects occur in the range $\delta_1 \approx 0.1$ to $\delta_1 \approx 0.15$ when the dot 1 is in the valence fluctuation regime. The shade for $\omega < 0$ in this range is the nascent molecular orbital state that becomes better defined for even larger t . The spectral weight in $A_1(\omega)$ for $\omega > 0$ is the disappearing atomic on-site orbital of dot 1 that eventually disappears for increased t . This is thus the *transient regime where both localized atomic and delocalized molecular spectral features coexist*.

Observing that interesting effects occur around $\delta_i \approx 0.1$, we now fix one of the dots to this value, i.e., $\delta_2 = 0.1$, and sweep the other in the full interval. At small t the second dot is in the VF regime and $A_2(\omega)$ shows a resonance near $\omega = 0$ which results from the merging of the Kondo resonance with the lower atomic peak. At intermediate value of $t = 10^{-2}$ we start to observe the effects of the exchange coupling: $A_2(\omega)$ shows a splitting of order J , see Fig. 6. In the central range $-0.1 < \delta_1 < 0.1$, there is consequently a non-negligible anti-ferromagnetic spin correlation $\langle \mathbf{S}_1 \cdot \mathbf{S}_2 \rangle \approx -0.1$. It is somewhat stronger for negative δ_1 , since in that case the overall occupancy is closer to 2, which is favorable for local singlet formation. As t grows, both spectral functions become visibly perturbed ($t = 2.15 \times 10^{-2}$, bottom row). The spin correlations in the centre are now much stronger, reaching values around -0.3 . The exchange splitting is asymmetric, which

can be explained by the following expression for J :

$$J = t^2 \left(\frac{1}{U/2 + \delta_1 - \delta_2} + \frac{1}{U/2 + \delta_2 - \delta_1} \right) \quad (3)$$

$$= \frac{4t^2}{U} \frac{1}{1 - 4(\delta_1 - \delta_2)^2/U^2},$$

which indicates that the largest exchange coupling is found for δ_i of opposite signs, here for $\delta_1 \sim -0.1$. The interdot coupling also affects the occupancy and charge fluctuations on dot 2: compared to the $t = 0$ values, the occupancy is increased (toward half-filling) in the $\delta_1 \sim 0$ region (charge fluctuations are little affected) and decreased near $\delta_1 \sim -0.1$ and $\delta_1 \sim 0.1$ points, where an increase of charge fluctuations is also observed. These results show that the behavior in this regime cannot be explained by the exchange coupling alone: the charge fluctuations also play an important role.

For large (absolute) values of δ_1 , the dot 1 becomes non-interacting, while the dot 2 returns to the single-impurity valence fluctuation regime with a resonance close to $\omega = 0$.

III. SUPERCONDUCTING ATOMIC LIMIT

Here we provide some additional details regarding the superconducting atomic (wide-gap) limit, introduced in Sec. II of the main text.

A. Eigenstates

The singlet space is spanned by the following five states (one from the zero-occupancy sector, three from the half-

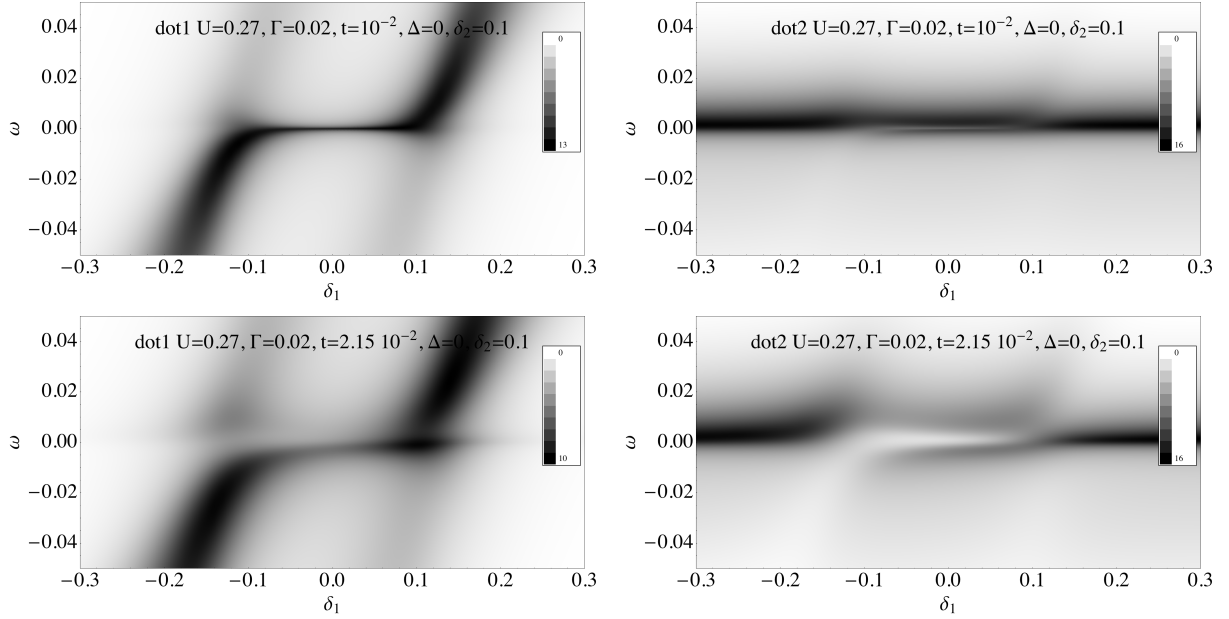


Figure 6: (Color online) Spectral function on dot 1 (left panels) and dot 2 (right panels) in the *normal* state for two values of the inter-dot couplings t . The quantum dot 2 is kept at $\delta_2 = 0.1$, which is in the *valence fluctuation regime*.

filling sector, and one from the full-occupancy sector)

$$\begin{aligned} &|0\rangle, \quad d_{2\downarrow}^\dagger d_{2\uparrow}^\dagger |0\rangle, \quad \frac{1}{\sqrt{2}} \left(d_{1\downarrow}^\dagger d_{2\uparrow}^\dagger - d_{1\uparrow}^\dagger d_{2\downarrow}^\dagger \right) |0\rangle, \\ &d_{1\downarrow}^\dagger d_{1\uparrow}^\dagger |0\rangle, \quad d_{1\downarrow}^\dagger d_{1\uparrow}^\dagger d_{2\downarrow}^\dagger d_{2\uparrow}^\dagger |0\rangle. \end{aligned} \quad (4)$$

$$H_S = \begin{pmatrix} U - \delta_1 - \delta_2 & \Gamma & 0 & \Gamma & 0 \\ \Gamma & U - \delta_1 + \delta_2 & -\sqrt{2}t & 0 & \Gamma \\ 0 & -\sqrt{2}t & 0 & -\sqrt{2}t & 0 \\ \Gamma & 0 & -\sqrt{2}t & U + \delta_1 - \delta_2 & \Gamma \\ 0 & \Gamma & 0 & \Gamma & U + \delta_1 + \delta_2 \end{pmatrix}. \quad (5)$$

In general, the eigenvalues cannot be expressed in (reasonably simple) closed form and need to be computed numerically. For $\delta_i = 0$ and $t = 0$, they are

$$0, U, U - 2\Gamma, U, U + 2\Gamma. \quad (6)$$

The first state is the inter-dot singlet with one electron on each dot. For $\delta = 0$, to lowest order in t only the first state shifts in energy by the superexchange coupling $4t^2/U$. For $t = 0$, to lowest order in δ the third and the fifth state shift to $U - 2\Gamma - \delta^2/\Gamma$ and $U + 2\Gamma + \delta^2/\Gamma$, respectively. When both δ and t are non-zero, the first state shifts down by the corresponding superexchange coupling $\propto t^2$, the third and the fifth shift by $\propto \delta^2$, while the two remaining states remain fixed at U . Since $U \gg \Delta$ in our NRG calculations, the states that are relevant for the sub-gap part of the spectrum are only two: the inter-dot singlet (first state) at $\approx -4t^2/U$, and the (third) state at $\approx U - 2\Gamma - \delta^2/\Gamma$ (denoted $|S1\rangle$ and $|S2\rangle$), respectively, in the

The Hamiltonian in this subspace is

main text).

The doublet space is spanned by the following four states (two each from single-occupancy and triple-occupancy sectors):

$$d_{2\uparrow}^\dagger |0\rangle, \quad d_{1\uparrow}^\dagger |0\rangle, \quad d_{1\uparrow}^\dagger d_{2\downarrow}^\dagger d_{2\uparrow}^\dagger |0\rangle, \quad d_{1\downarrow}^\dagger d_{1\uparrow}^\dagger d_{2\uparrow}^\dagger |0\rangle. \quad (7)$$

The corresponding Hamiltonian is

$$H_D = \begin{pmatrix} \frac{U}{2} - \delta_1 & -t & 0 & \Gamma \\ -t & \frac{U}{2} - \delta_2 & \Gamma & 0 \\ 0 & \Gamma & \frac{U}{2} + \delta & t \\ \Gamma & 0 & t & \frac{U}{2} + \delta_1 \end{pmatrix}. \quad (8)$$

The corresponding eigenstates are discussed in the main text.

The triplet state has energy 0 irrespective of the parameters.

B. Shiba state level diagrams

We proceed in the order in which the NRG results are presented in the main text. In Fig. 7(a) we consider the left-right symmetric case at half-filling for increasing inter-dot coupling t . This should be compared with the bottom panel in Fig. 3 in the main text. The lowest three states are in direct correspondence: the ground state is always the inter-dot singlet state, there is a triplet state growing in energy as $\propto 4t^2/U$, and a doublet excited state. The singlet-triplet splitting behaves similarly in both approaches. There are more differences related to the doublet state: at $t = 0$, in the NRG we find it at $\Omega = 0.6\Delta = 0.006$ while here it is found at a much higher energy of $\approx U/2 - \Gamma$. Nevertheless, we find the same increasing trend at large t , thus qualitative behavior is the same. The remaining states are irrelevant for our purposes since they are merged with the continuum; this is also the case in all following examples.

In Fig. 7(b) we study the $\delta = \delta_1 = \delta_2$ dependence at constant t . These results should be compared with the diagrams in Fig. 8 of main text. There is an important qualitative difference here: the NRG shows that the ground state is always a singlet and that there is an avoided level crossing between the two singlet Shiba states, yet in the atomic limit we find a finite parameter range where one of the doublet states becomes the ground state and, furthermore, there is a crossing of the singlet states in the same parameter range. This indicates that the avoided crossing in the true solution is due to virtual transitions through the quasiparticle continuum. (For large Δ , we find the intermediate doublet ground state also in the NRG solution, confirming the important role of the quasiparticles.)

In Fig. 7(c) we consider the asymmetric case with δ_2 fixed to 0 and variable δ_1 , to be compared with the Shiba level diagram in Fig. 12 in main text. It correctly reproduces the splitting of the doublet states at low δ_1 , the singlet-doublet quantum phase transition induced by driving one of the dots away from the Kondo regime toward the empty orbital regime, as well as the behavior of the triplet state.

Finally, in Fig. 7(d) we plot the generic case with the QD2 in the valence fluctuation regime, to be compared with the Shiba level diagrams in Fig. 13 in main text. The quantum phase transition at $\delta_1 \approx 0.1$ is correctly reproduced, while the one at $\delta_1 \approx -0.15$ occurs in the true solution only at much lower δ_1 .

C. Deviations from the wide-gap limit

Here we briefly consider the main effects of finite gaps compared to the wide-gap limit. For $\Delta \rightarrow \infty$ the continuum of the quasiparticle states plays no role, thus there is strictly speaking no Kondo physics and the only effect of the superconducting lead is the proximity effect, i.e., a local pairing field proportional to the hybridization strength Γ . The singlet-doublet transition is then simply due to the occupancy variation: there are two singlet states with energies

$$\frac{U}{2} \pm \sqrt{\Gamma^2 + \delta^2}, \quad (9)$$

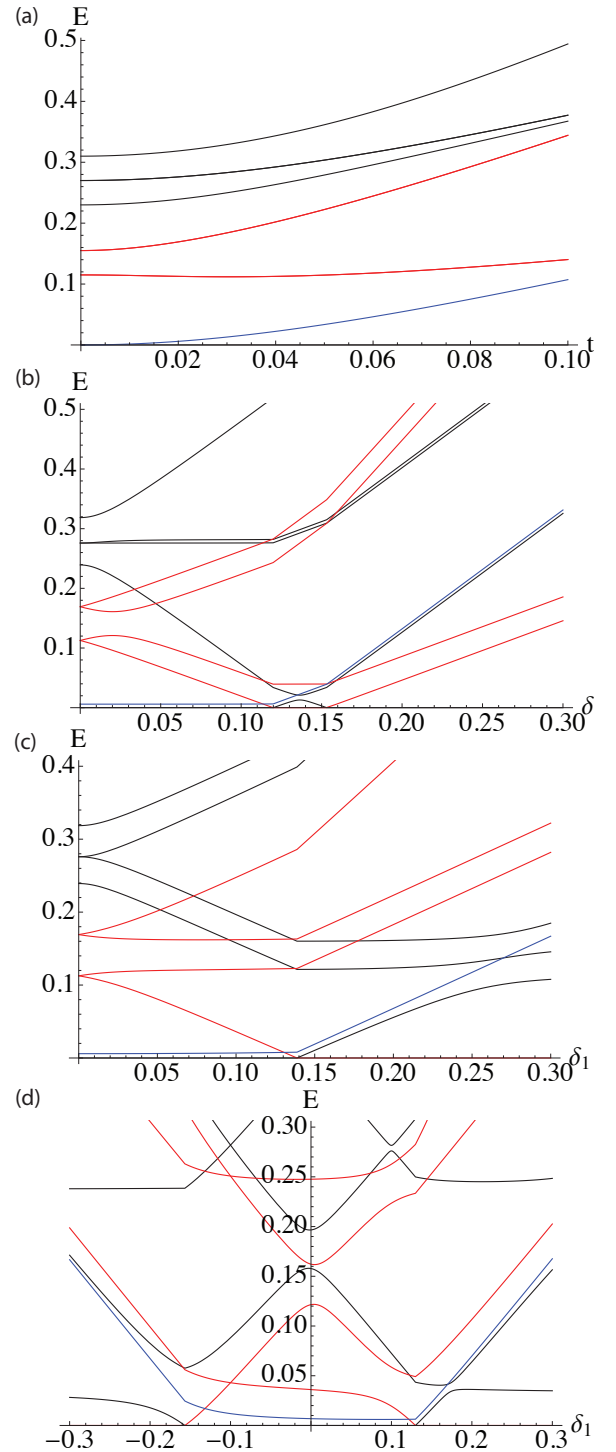


Figure 7: (Color online) Eigenvalues of the effective Hamiltonian in the superconducting atomic limit ($\Delta \rightarrow \infty$). The color scheme is the same as for the NRG results: black lines are $S = 0$, red lines $S = 1/2$, blue line is $S = 1$. a) Left-right symmetric case, half-filling, evolution as a function of t . b) Left-right symmetric case away from half-filling, $t = 0.02$. The singlet states (black lines) actually cross, the appearance of avoided crossing is a plotting artifact. c) Generic case with $\delta_2 = 0$, $t = 0.02$. d) Generic case with $\delta_2 = 0.1$, $t = 0.02$. In all calculations $U = 0.27$, $\Gamma = 0.02$.

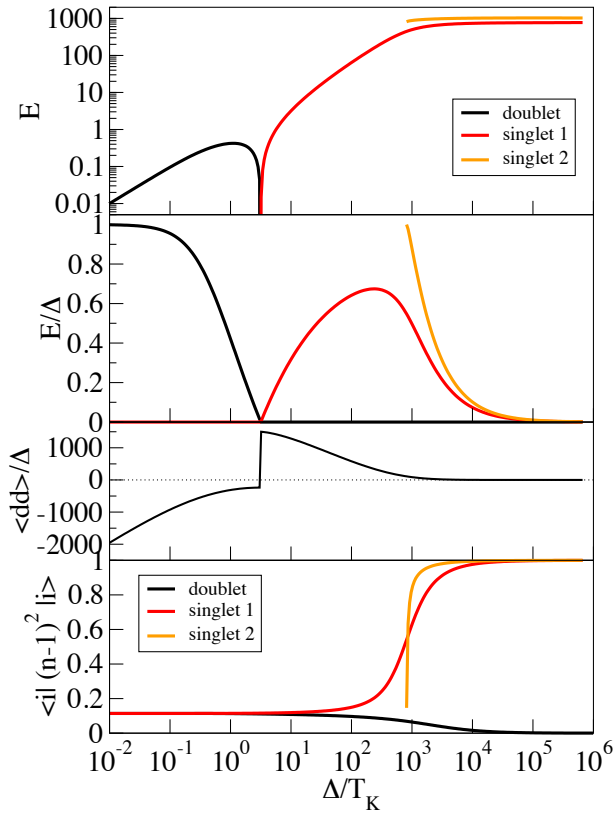


Figure 8: (Color online) Single quantum dot case at the particle-hole symmetric point, $\delta = 0$, for fixed U and Γ and variable Δ . (a) Sub-gap state energies showing the singlet-doublet transition at $\Delta \approx 3T_K$. (b) Sub-gap state energies rescaled with the gap Δ . The second singlet state enters the sub-gap region only at very large $\Delta \sim 10^3 T_K$. (c) Ground state expectation value of the pairing operator, rescaled by Δ . (d) Charge fluctuations in the sub-gap Shiba states, evaluated as the expectation values of the corresponding many-particle states. The parameters are: $U/\Gamma = 0.27/0.02$.

and a doublet at zero energy. In the opposite limit of $\Delta \rightarrow 0$, there is no superconductivity, only Kondo screening. The cross-over between the two regimes occurs for $\Delta \sim T_K$.

At the particle-hole symmetric point and for fixed U , T_K is constant and Δ can be tuned across the singlet-doublet quantum phase transition, see Fig. 8. The asymptotic superconducting atomic limit regime with both singlet excitations present inside the sub-gap region occurs only for very large $\Delta/T_K \gtrsim 10^3$. This scale is determined by $\Delta \sim U$, i.e., *the superconducting atomic limit is reached when the energy scale of the atomic processes is comparable or lower than the superconducting gap*. This cross-over is unrelated to Kondo physics, as evident from the large separation of the relevant energy scales. The most interesting information about this cross-over is contained in the charge fluctuations of the singlet states, shown in the bottom panel. The cross-over to the atomic limit corresponds to a change in the nature of the singlet states from delocalized Kondo singlets formed by the local moment on the quantum dot and the conduction-band electrons (hence charge fluctuations are low and determined by the ratio of the hybridization strength over e-e repulsion, Γ/U), to BCS like singlet states $1/\sqrt{2}(|0\rangle \pm |\uparrow\downarrow\rangle)$ with saturating charge fluctuations that are caused by the proximity effect, not by quasiparticle hopping. (In the NRG, the information about the expectation values of all sub-gap states is directly available in a reliable way through the diagonal matrix elements of the corresponding singlet operators^{3,4}.)

The general trend of Δ decreasing from the $\Delta \rightarrow \infty$ (atomic) limit can be generalized: it leads to a decreasing energy of states associated with the Kondo screening. In the DQD case, these are chiefly the two doublet states, as well as the first excited singlet state.

¹ B. A. Jones, C. M. Varma, and J. W. Wilkins, Phys. Rev. Lett. **61**, 125 (1988).

² G. Zaránd, C.-H. Chung, P. Simon, and M. Vojta, Phys. Rev. Lett. **97**, 166802 (2006).

³ R. Žitko, O. Bodensiek, and T. Pruschke, Phys. Rev. B **83**, 054512 (2011).

⁴ D. Golež, J. Bonča, and R. Žitko, Phys. Rev. B **86**, 085142 (2012).